THE JOURNAL OF PHYSICAL CHEMISTRY B

Article

pubs.acs.org/JPCB

Mechanistic Study of Bleach-Imaged Plasmon Propagation (BlIPP)

David Solis, Jr.,[‡] Aniruddha Paul,[†] Wei-Shun Chang,[†] and Stephan Link*[,†,‡]

[†]Department of Chemistry, and [‡]Department of Electrical and Computer Engineering, Laboratory for Nanophotonics, Rice University, Houston, Texas 77005, United States

Supporting Information

ABSTRACT: Bleach-imaged plasmon propagation, BlIPP, is a far-field microscopy technique developed to characterize the propagation length of surface plasmon polaritons in metallic waveguides. To correctly extract the propagation length from the measured photobleach intensity, it is necessary to understand the mechanism by which dye photobleaching occurs. In particular, 1- vs 2-photon bleaching reactions yield different propagation lengths based on a kinetic model for BlIPP. Because a number of studies have reported on the importance of 2-photon processes for dye photobleaching, we investigate here the nature of the photobleaching step in BlIPP. We are able to demonstrate that only 1-photon absorption is relevant for typical BlIPP conditions as tested here for a thin film of indocyanine green fluorescent dye molecules coated over gold nanowires and excited at a wavelength of 785 nm. These results are obtained by directly measuring the excitation intensity dependence of the photobleaching rate constant of the dye in the presence of the metallic waveguide.

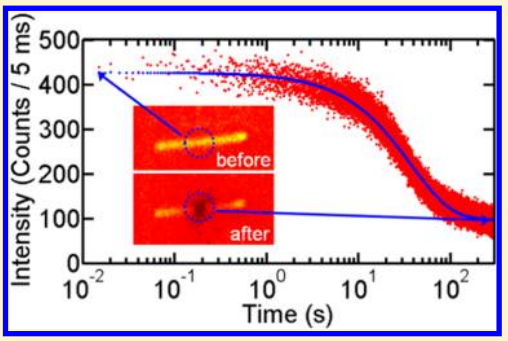

INTRODUCTION

Subwavelength wide plasmonic waveguides have the ability to confine electromagnetic energy on length scales below the diffraction limit and to transfer this energy over distances much larger than the lateral size of the waveguide through coupling of incident light to coherent oscillations of the free electrons, known as surface plasmon polaritons.[1−6] Metallic waveguides are, however, inherently prone to loss, and many studies have been aimed at understanding and minimizing these unwanted losses. Examples include controlling the waveguide morphology and crystallinity,[7−11] optimizing light coupling schemes,[12,13] and using metamaterials[14] and different surface coatings.[15−18] The damping of a surface plasmon polariton is characterized by an exponential decay of the near-field intensity from the point of optical excitation. This plasmon propagation length, L_0, has been measured through several methods such as near-field scanning optical microscopy,[12,19] leakage radiation microscopy,[9,15,20] and far-field fluorescence microscopy including direct fluorescence imaging[21,22] and its inverse analogue bleach-imaged plasmon propagation (BlIPP).[23−25]

In fluorescence microscopy methods, a thin film of a fluorescent dye or polymer is coated on top of the plasmonic waveguide and indirect excitation of the chromophore by the near-field of the propagating surface plasmon polariton is read out by a standard far-field microscope. Direct fluorescence imaging and BlIPP are in many aspects complementary to each other and have different advantages. Direct fluorescence imaging is usually carried out by imaging the fluorescence intensity directly on a CCD camera to spatially resolve the fluorescence intensity along the plasmonic waveguide while exciting one end with a laser. This method is characterized by short acquisition times and allows multiple measurements on the same waveguide. However, the laser excitation itself creates a strong fluorescence background that, especially for short propagation distances, can completely mask weaker fluorescence induced by the plasmonic near-field. Photobleaching of the dye film for high laser excitation intensities and long or repeated exposure times can also potentially affect the measured plasmon propagation length.

BlIPP, on the other hand, utilizes the photobleaching of the fluorescent molecules to create a permanent map of the plasmonic near-field, which is then read out by a low intensity, nondestructive probe beam. Because direct photobleaching by the excitation laser stops when all dye molecules are bleached, short propagation lengths as well as weak modes can be amplified in comparison, as indirect photobleaching through the plasmonic near-field continuously increases with increasing exposure time. Furthermore, by taking into account the spatial intensity profile of the excitation beam, BlIPP has successfully been used to record plasmon propagation lengths shorter than 2 μm in gold nanowires (Au NW) excited at 532 nm.[23] However, as with other indirect detection schemes, the correct extraction of the plasmon propagation length using BlIPP strongly depends on the underlying mechanism of the dye photobleaching reaction on top of the plasmonic waveguide structures. In previous BlIPP studies, the photobleaching mechanism was assumed to be based on a one-photon

Special Issue: Paul F. Barbara Memorial Issue

Received: September 4, 2012
Revised: November 26, 2012

   dx.doi.org/10.1021/jp308790m | J. Phys. Chem. B XXXX, XXX, XXX−XXX

process,[23−25] although at high excitation intensities two-photon induced photobleaching is also possible.[26−28]

In this study we examine in detail the photobleaching reaction in BlIPP measurements and its effect on the determination of the plasmon propagation length. We first present a kinetic model describing the measured signal intensity in BlIPP and then take a closer look at the excitation intensity, I, dependence of the photobleaching rate constant, k_{bl}. In particular, we investigate if photobleaching on top of a Au NW occurs solely via one-photon absorption or whether two-photon absorption also plays a role as these two photobleaching mechanisms give plasmon propagation lengths that differ by a factor of 2. This is important because both 1- and 2-photon photobleaching reactions are well-documented in the literature.[26−29] We therefore determined k_{bl} as a function of I, where a 1-photon process should give a linear relationship between k_{bl} and I, whereas a 2-photon process should show a quadratic dependence with k_{bl} being proportional to I^2.[26,28]

MATERIALS AND EXPERIMENTAL SETUP

Samples were prepared by first drop casting a solution of CTAB (cetyltrimethylammoniun bromide) capped Au NWs (10−15 μm long with a diameter of 90 ± 10 nm) onto a clean glass coverslip. Excess CTAB was removed from the substrate by washing with ethanol followed by drying under a nitrogen flow. The Au NWs were synthesized via tip selective growth of purified pentahedrally twinned gold nanorods, a method which has been shown to produce smooth, highly crystalline NWs.[25,30] The Au NWs were coated with a thin dye film, which was created by spin coating 30 μL of a 0.5 mg/mL indocyanine green (ICG, Sigma Aldrich) solution in methanol onto a glass coverslip decorated with Au NWs at 6000 rpm for 50 s. The dye film thickness was measured to be 5 ± 1 nm as determined by atomic force microscopy (Veeco).[25] This sample was then placed on a home-built confocal fluorescence microscope, which used a diode laser (Power Technology) with an operating wavelength of 785 nm for the measurements reported here. Circular polarized light with a ratio of the minor polarization axis to the major polarization axis >0.6 was used and the laser intensity was varied using neutral density filters. The small degree of elliptical polarization had no effect on the fluorescence enhancement and dye photobleaching. The laser beam was directed into the body of an inverted microscope (Zeiss) where it was reflected by a dichroic mirror into a 50× objective (numerical aperture of 0.8) and focused onto the dye coated side of the Au NW sample, which was attached to a XYZ piezo scanning stage (Physik Instrumente). Fluorescence from the excited dye molecules was then collected by the same objective in an epi-fluorescence geometry and focused onto an avalanche photodiode detector (Perkin-Elmer). Fluorescence images were acquired by scanning the sample with the piezo stage which was controlled by a surface probe microscope controller (RHK Technology).[31] Fluorescence intensity time transients were collected on a separate counter board (Becker & Hickl). Fluorescence intensity data and image processing were performed using Matlab. The beam waist of the focused laser at the sample, as defined by the diameter measured at the $1/e^2$ intensity values, was measured to be 1000 ± 60 nm using the confocal scattering signal from individual gold nanorods and was used to calculate the excitation intensity per unit area.

RESULTS AND DISCUSSION

BlIPP at 785 nm is demonstrated in Figure 1 for Au NWs overcoated with ICG. A fluorescence image of the dye emission

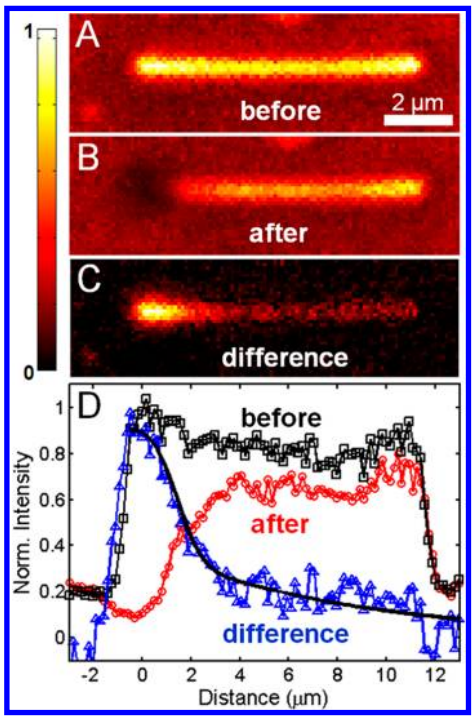

Figure 1. Bleach-imaged plasmon propagation (BlIPP). (A) Sample scanned confocal fluorescence image of an Au NW coated with ICG dye excited at 785 nm using a laser intensity of 8.0 W/cm^2. (B) Fluorescence image of the same area after irradiating with a laser intensity of 1.25 kW/cm^2 at the left end of the NW for 20 min. (C) Difference image obtained by subtracting (B) from (A) yielding the bleach intensity. (D) Width-averaged intensity line-sections along the long NW axis shown for before (black squares) and after (red circles) photobleaching as well as the beach intensity line section (blue triangles) extracted from the difference image, where each point of the difference line-section has been normalized to its corresponding point in the fluorescent image before photobleaching. The black line is a fit to eq 7 yielding a propagation length of L_0 = 7.5 ± 1.0 μm.

was first collected at a low excitation intensity by scanning the sample over a tightly focused laser beam. This low excitation intensity was found to cause negligible photobleaching as evaluated in Figure S1. The fluorescence of the ICG molecules was enhanced on top of the Au NW due to coupling to the NW plasmon modes.[31,32] The image in Figure 1A shows the Au NW on top of background fluorescence. The Au NW was then positioned in such a way that the same excitation laser was exciting one of the NW ends (the left end for Figure 1) at a higher excitation intensity. Because of symmetry breaking at the NW end the laser can couple to propagating surface plasmon modes, which decay exponentially along the NW due to mostly intrinsic nonradiative damping.[6,19,33,34] The near-field of the propagating plasmon modes, however, also excited the ICG molecules, which, due to their limited photostability, photobleached as the end-excitation was continued for 20 min. This photobleaching was then measured by acquiring another fluorescence image (Figure 1B) with the original lower excitation intensity. Because photobleaching also occurred from direct laser excitation at the NW end, it is easier to visualize the degree of photobleaching along the NW by

dx.doi.org/10.1021/jp308790m | J. Phys. Chem. B XXXX, XXX, XXX−XXX

creating a difference image (Figure 1C). The photobleach intensity averaged over the width of the NW as shown in Figure 1D (blue data points) is then used to extract the plasmon propagation length, L_0. For Au NWs as the one shown in Figure 1, we previously obtained an average propagation length of $\langle L_0 \rangle = 7.5 \pm 2.0$ μm, which corresponds to the higher order $m = 1$ mode because the fundamental $m = 0$ mode is quenched under these experimental conditions.[25]

BlIPP is based on photobleaching, which renders the dye molecule nonemissive after repeated absorption and emission cycles. In addition to the radiative process of emission, which typically occurs from the lowest excited singlet state, an excited molecule can also relax nonradiatively to the ground state or relax into a dark triplet state.[35,36] While in the triplet state, aided by its longer lifetime, the molecule can undergo an irreversible reaction effectively turning off the fluorescence. In many cases it is oxygen which reacts with the photoexcited molecule in its triplet ground state. This photobleaching mechanism can be described by a 3-level system[29,37] which requires the absorption of only one photon. However, at high excitation intensities it has been shown that a 5-level system[29,38] or 2-photon photobleaching mechanism may dominate, where the molecule in the triplet state first absorbs a second photon before undergoing an irreversible chemical reaction, or the molecule may absorb a second photon while in the first excited state and then undergoes intersystem crossing from the excited singlet state to an excited triplet state, followed again by an irreversible chemical reaction. This 2-photon absorption brings the molecule to a more reactive higher energy triplet state, thereby increasing the likelihood of a photobleaching event to occur. The photobleaching rate constant, k_{bl}, therefore depends on the excitation intensity: in the case of a 1-photon process, $k_{bl} \propto I$, whereas for the 2-photon mechanism, $k_{bl} \propto I^2$.[26,28] This difference in excitation intensity dependence of the photobleaching reaction may lead to an erroneous estimation of the propagation length in plasmonic waveguides using BlIPP. We show first how the type of photobleaching reaction leads to different propagation lengths by presenting in detail the derivation of the rate equation model used to fit the photobleach intensity in Figure 1D and then experimentally determine whether photobleaching in our BlIPP measurements occurs via a 1- or 2-photon pathway.

Assuming a first order reaction, the fluorescence intensity, F, at time, t, can be expressed by eq 1, where F_0 is the initial fluorescence intensity at time zero.

$$F(t) = F_0 \exp(-k_{bl}t) \tag{1}$$

For a spatially varying excitation intensity, $I(x)$, with the direction along the plasmonic waveguide taken to be the x direction and considering first a one photon reaction, k_{bl} can be written as given by eq 2.

$$k_{bl} = k_0 I(x) \tag{2}$$

where k_0 represents the product of several intrinsic properties of the dye, including the composite microscopic rate constants of photobleaching from all possible excited states, the absorption cross section, and the radiative rate constant.[27,29] Substituting eq 2 into eq 1 and rearranging eq 1, we can write the ratio of fluorescence intensities at time t over the initial fluorescence intensity as a function of position x according to eq 3.

$$\frac{F(t)}{F_0} = \exp(-k_0(I_G(x) + I_{SPP}(x))t) \tag{3}$$

Here $I_G(x)$ is the spatial intensity distribution of the Gaussian laser beam with σ describing its width and centered at the point of excitation ($x = 0$), which corresponds to the center of the laser exciting the NW end, as given by eq 4. $I_{spp}(x)$ is the spatial intensity distribution of the near-field of the propagating surface plasmon wave that can be described by a exponential decay curve with propagation length, L_0, according to eq 5.

$$I_G(x) = I_{G,0}e^{-x^2/2\sigma^2} \tag{4}$$

$$I_{SPP}(x) = I_{SPP,0}e^{-x/L_0} \tag{5}$$

$I_{G,0}$ and $I_{SPP,0}$ are the maximum intensities at $x = 0$. Upon substitution of eqs 4 and 5 into eq 3, we obtain eq 6, which describes the fluorescence intensity normalized by the initial fluorescence intensity as a function of time t and position x.

$$\frac{F(t)}{F_0} = \exp(-t(k_0 I_{G,0}e^{-x^2/2\sigma^2} + k_0 I_{SPP,0}e^{-x/L_0})) \tag{6}$$

The photobleach intensity measured by BlIPP is then given by subtracting eq 6 from the value of 1, the initial fluorescence intensity in this normalized equation. This yields eq 7, which describes the intensity of fluorescence bleaching at time t and position x.

$$I_{bl}(x, t) = 1 - \exp(-t(k_0 I_{G,0}e^{-x^2/2\sigma^2} + k_0 I_{SPP,0}e^{-x/L_0})) \tag{7}$$

Equation 7 well describes the BlIPP data as verified by performing time-dependent measurements.[23,25] The propagation length, L_0, is then determined by fitting the width-averaged line-section of the photobleach intensity along the NW (x direction) to eq 7 (see the black line in Figure 1D). The coefficients, $k_0 I_{G,0}$ and $k_0 I_{SPP,0}$, are treated as variables, typically within a fairly narrow range of ~20% ($1.2 \times 10^{-3} \pm 2.2 \times 10^{-4}$ s^{-1} and $4.1 \times 10^{-4} \pm 0.8 \times 10^{-4}$ s^{-1}, respectively) to achieve the best agreement between the fit and the experimental data from NW to NW. Small variations can be explained by differences in the local film thickness, which is expected to lead to changes in $I_{G,0}$ as the intensity is modified by the absorption of individual and aggregated dye molecules, and considering the fact that the shape of the NW tips often varies, therefore affecting the coupling efficiency between photons with the propagating plasmons and hence $I_{SPP,0}$. The width of the Gaussian laser profile, σ, was obtained separately by performing BlIPP experiments on dye coated glass coverslips where no NWs were present. In those experiments the bleach intensity line-section was described by only the Gaussian intensity profile of the laser resulting in values of $\sigma = 1.5 \pm 0.2$ μm. In our fitting routine σ was then adjusted within this range of the experimental error. It should be noted that σ of the Gaussian intensity profile for the photobleaching was slightly larger than the excitation beam spot profile itself (see the Materials and Experimental Setup section) because scattered light from the NW end and the glass substrate might also contribute to photobleaching of the dye.

Equation 7 follows from a 1-photon photobleaching mechanism, but as mentioned above, at higher excitation intensities 2-photon pathways are also possible.[29] Instead of eq 2 we now have to consider that the photobleaching rate constant depends on the square of the excitation intensity

dx.doi.org/10.1021/jp308790m | J. Phys. Chem. B XXXX, XXX, XXX−XXX

according to eq 8, which then results in eqs 9 and 10 following the same derivation as outlined above for eq 7.

$$k_{bl} = k_0 I^2(x) \tag{8}$$

$$\frac{F(x)}{F_0} = \exp(-k_0(I_G(x) + I_{SPP}(x))^2 t) \tag{9}$$

$$I_{bl}(x, t) = 1 - \exp(-k_0 t(I_{G,0}{}^2 e^{(-x^2/\sigma^2)} + 2I_{G,0}I_{SPP,0}e^{(-x^2/2\sigma^2 + -x/L_0)} + I_{SPP,0}^2 e^{\left(\frac{-x}{\left(\frac{L_0}{2}\right)}\right)})) \tag{10}$$

Away from the point of laser excitation (large x values) the first two terms in eq 10 become very small so that the contribution from the surface plasmon intensity dominates the bleaching intensity. Equation 10 can hence be simplified as given by eq 11.

$$I_{bl,large\,x}(x, t) = 1 - \exp(-t(k_0 I_{SPP,0}{}^2 e^{-x/(L_0/2)})) \tag{11}$$

The difference between eqs 7 and 11 is the factor of 2 in the denominator of the exponential, which means that, if a 2-photon process dominates the photobleaching mechanism in a BlIPP measurement, the true propagation length of the plasmonic waveguide would be twice of the value that is obtained with eq 7. It is therefore important to experimentally verify if the primary photobleaching mechanism in BlIPP occurs via a 1- or 2-photon process. We therefore measured the photobleaching rate constant, k_{bl}, as a function of excitation intensity both on single Au NWs and on areas on the glass coverslip where only dye molecules were present.

To measure k_{bl} for the dye photobleaching on the Au NW we positioned the stage such that the laser was focused onto a single NW. The middle region of an Au NW was chosen to minimize the effect of enhanced scattering at the NW tips while still probing the dye fluorescence enhanced by the metal. The integrated fluorescence intensity for the chosen sample position was measured with a single element avalanche photodiode detector as a function of time using a photon counting board set to a time resolution of 5 ms and a total acquisition time of 5 min. This experiment was repeated for different Au NWs and different excitation intensities, which were comparable to the values used for BlIPP. The same measurements were then carried out under identical conditions with the sample positioned so that the laser excited a background area where no Au NW was present, but where strong fluorescence from the continuous dye film could be observed. The fluorescence images in Figure 2A,B illustrate these experiments by showing a sample area with a Au NW before and after localized photobleaching was performed on top of the NW as well as next to it. Figure 2C shows a typical example of a fluorescence transient recorded on top of a Au NW with an excitation intensity of 1.2 kW/cm^2. The decrease in the fluorescence intensity with time is due to laser induced photobleaching.

Each fluorescence transient as the one shown in Figure 2C was best described by a biexponential decay instead of the monoexponential behavior given by eq 1.[27] We assign the fast component, k_1, of the fitted biexponential curve to the photobleaching rate constant of the dye, k_{bl}. The 5 ms bin time did not allow us to resolve fast photoblinking events from single molecules, which would have also been averaged out by the high dye concentration of the film.[27,39,40] The second slow photobleaching component, k_2, originates from the spatially

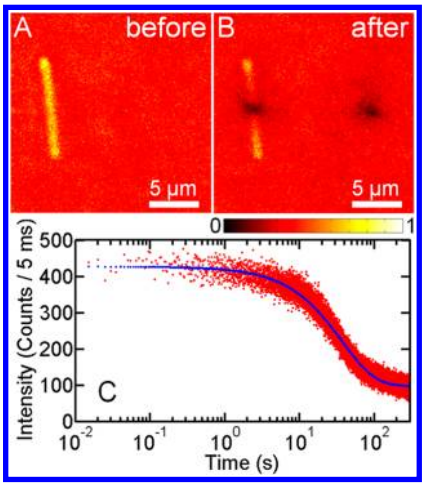

Figure 2. (A) Fluorescence image of a 20 μm × 20 μm area containing a Au NW acquired with a low excitation intensity of 7.8 W/cm^2 (B) Fluorescence image of the same area recorded after measuring k_{bl} in the middle of the NW and in a background area to the right of the NW at a laser intensity of 1.2 kW/cm^2. (C) Fluorescence intensity observed on top of a Au NW as a function of time. The laser excitation intensity was 1.2 kW/cm^2 at 785 nm. The experimental data is shown in red and a biexponential fit with decay constants of $k_1 = 3.1 \times 10^{-2}$ s^{-1} and $k_2 = 2.7 \times 10^{-3}$ s^{-1} is given by the blue line. k_1 is assigned to k_{bl}.

varying Gaussian excitation beam. In a theoretical treatment, Berglund[41] has shown that photobleaching by an excitation source with a spatially varying intensity profile such as a Gaussian laser beam follows a nonexponential behavior independent of the underlying mechanism (1- vs 2-photon) but can be described by a sum of exponential decay functions. For the present case, we have chosen the simplest version of a sum of two exponential decays, where the fast component represents the photobleaching of the dye molecules in close proximity to the Gaussian beam center, while the slow component corresponds to photobleaching of the dye molecules at the edges of the laser spot where the excitation intensity is much lower. This approach is consistent with the fact that in these experiments with the single element detector without scanning the sample, no spatial information was obtained as with the BlIPP measurements. The spatially integrated signal was chosen because we were able to acquire the fluorescence transients with a higher time resolution compared to imaging. Another explanation for the nonexponential decay of the fluorescence intensity in Figure 2C is that nonuniformities in the dye concentration of the thin film may also lead to heterogeneities in the observed photobleaching dynamics, as reported previously.[42,43] The assignment of k_1 to k_{bl} is furthermore consistent with the observation that the decay times fitted for the slow component, k_2, varied randomly within the range of 8−20 min.

A linear relationship of k_{bl} with excitation intensity verifies a 1-photon photobleaching mechanism of BlIPP for this system of plasmonic waveguide and dye. Figure 3A,B summarizes the values of k_{bl} obtained for all experiments carried out on top of the Au NWs (A) and for the dye film only (B) as a function of excitation intensity. The error bars were calculated as the standard deviation from at least 8 measurements on 7 independent samples. The trends in Figure 3A,B show a linear relationship in agreement with eq 2, establishing that the photobleaching mechanism of the ICG dye film used in these

dx.doi.org/10.1021/jp308790m | J. Phys. Chem. B XXXX, XXX, XXX−XXX

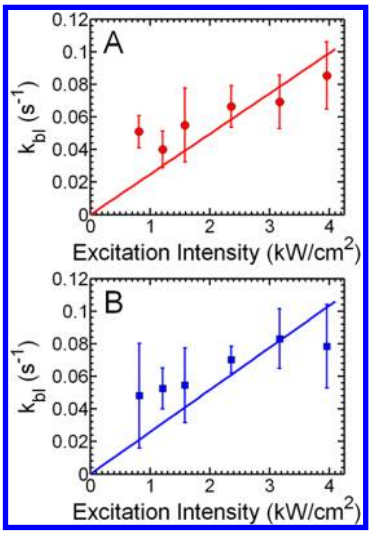

Figure 3. Intensity dependence of the photobleaching rate constant k_{bl}. (A) Dependence of k_{bl} on the excitation intensity measured for the plasmon enhanced fluorescence on top of Au NWs. (B) Same as in panel A but measured in the background near the Au NWs, where the dye is deposited only on glass. k_{bl} was obtained as the first component of a biexponential fit to time transients such as the one shown in Figure 2C. The solid lines in panels A and B are linear fits to the data points based on eq 2. For each intensity, the measurements were repeated at least 8 times and the error bars represent the standard deviation. The variation in the values for k_{bl} are likely due to local difference in the dye film.

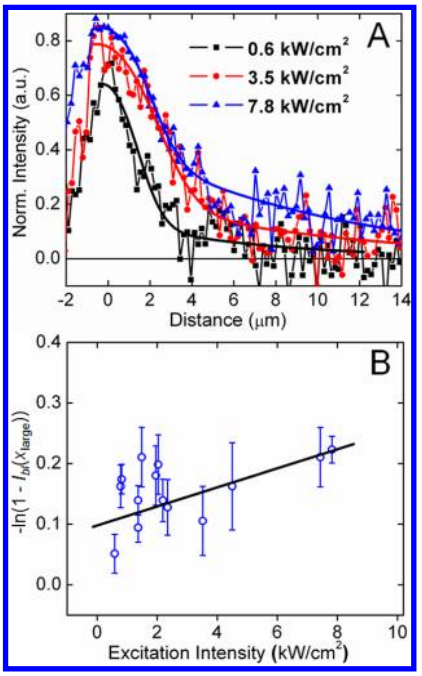

Figure 4. Intensity dependence of BlIPP at exposure time, t = 20 min. (A) Width-averaged bleach intensity line-sections along the long NW axis as extracted from the difference images for three different Au NWs exposed to laser intensities of 0.6, 3.5, and 7.8 kW/cm^2 with fits (lines) according to eq 7. (B) Laser excitation intensity dependence of the bleach intensity according to eq 13 measured for Au NWs excited with a 785 nm laser at x_{large} = 8.5 μm away from the NW tip that was exposed during the BlIPP measurements. Each data point was measured for a different Au NW and extracted from the corresponding width-averaged bleach intensity line-section, such as those shown in panel A. The error bars were estimated from individual BlIPP traces, by calculating the average deviation of ±3 data points from the central data point.

BlIPP studies is based on a 1-photon process. Fits associated with the 2-photon photobleaching mechanism (eq 8) are given in Figure S2 and fail to describe the experimental data. Furthermore, the slopes of the linear fits in Figure 3A,B are identical within the error bounds at a value of 2.5×10^{-2} $s^{-1}/(kW/cm^2)$. This last conclusion indicates that, although the fluorescence is enhanced over the Au NWs, coupling between the dye molecules and the plasmonic near-field has no or little effect on the photobleaching rate constant, k_{bl}, and hence the chemical reaction causing the photobleaching.

Further experimental verification of the 1-photon photobleaching mechanism was obtained by comparing BlIPP experiments carried out for different Au NWs as a function of excitation intensity. Using the bleach intensity recorded by BlIPP instead of direct laser excitation measurements as in Figures 2 and 3 allows for the observation of the intensity dependent photobleaching due to the indirect excitation of the dye molecules via the propagating surface plasmon near-field. Figure 4A shows the width-averaged line-sections from the difference images of three different Au NWs measured by BlIPP at 0.6, 3.5, and 7.8 kW/cm^2. This comparison is important because photobleaching by the plasmonic near-field occurs on much slower time scales compared to direct laser excitation and it was difficult to access such a low excitation intensity regime in Figure 3 with direct laser excitation as the measurement noise increased dramatically with lower laser intensities. The bleach intensity line-sections in Figure 4A demonstrate that an increase in the excitation intensity increases the total bleach intensity signal along each Au NW. For the first 3 μm closest to the point of laser excitation it appears that the two higher excitation intensities have caused saturation of the photobleach intensity. Photobleaching in this region is dominated by direct photobleaching by the incident laser, whereas photobleaching far from the point of excitation along the NW is most indicative of the excitation intensity dependent coupling and bleaching of the dye molecules by the near-field of the propagating plasmon modes.

To quantitatively analyze the excitation intensity dependence of the BlIPP signal in Figure 4A, we first rewrite eq 7 according to eq 12 to demonstrate the exponential relationship of the photobleach intensity I_{bl} with the excitation intensity at a given position, x, along the NW.

$$-\ln(1 - I_{bl}(x, t)) = tk_0(I_G(x) + I_{SPP}(x)) \quad (12)$$

In Figure 4B, we therefore plot $-\ln(1 - I_{bl}(x,t))$ at a given exposure time, t = 20 min, and at a large distance of x_{large} = 8.5 μm away from the excited NW tip as a function of laser excitation intensity, where we assume that I_{SPP} is directly proportional to the laser intensity. At distances far from the point of excitation, the contribution of the Gaussian excitation beam approaches zero, which means that eq 12 can be further simplified as given by eq 13.

$$-\ln(1 - I_{bl}(x_{large}, t)) = tk_0(I_{SPP}(x_{large})) \quad (13)$$

The data shown in Figure 4B was collected from 15 NWs. The spread in measured values is likely due to the fact that each measurement at a different excitation intensity had to be carried out on another NW with a slightly different tip geometry and width, which both influence the coupling efficiency of the excitation light to the propagating surface plasmon modes and

dx.doi.org/10.1021/jp308790m | J. Phys. Chem. B XXXX, XXX, XXX–XXX

hence cause variations in I_{SPP}. Nevertheless, the dependence of the dye photobleaching on the intensity of the surface plasmon near-field follows the linear trend given by eq 13, i.e., $-\ln(1 - I_{bl}(x,t))$ linearly depends on $I_{SPP}(x)$, rather than a quadratic relationship scaling with $(I_{SPP}(x))^2$. Bleach intensities were furthermore evaluated at $x = 5$ μm and $x = 10$ μm as shown in Figure S3, and the same linear dependence as in the case of $x = 8.5$ μm is observed. These results indicate that both direct excitation of the dye by the laser and indirect excitation by the near-field of the propagating plasmons follow a 1-photon photobleaching mechanism.

CONCLUSIONS AND OUTLOOK

In conclusion, we have investigated the excitation intensity dependence of the photobleaching reaction that gives rise to the signal in BlIPP. Our experimental results show that photobleaching of the dye ICG coated over Au NWs occurs via a 1-photon photobleaching mechanism. It is important to establish the dye photobleaching mechanism, as the kinetic model developed for BlIPP predicts that a 2-photon process would lead to a propagation length that is larger by a factor of 2. Our results also show that the coupling between the dye molecules and the plasmonic near-field has no or little effect on the chemical reaction responsible for the photobleaching. Furthermore, it is worth pointing out that with the values determined for the photobleaching rate constant, k_{bl}, under the conditions evaluated here for ICG molecules, it should be possible to extract from the fitting values the initial intensity of the excited surface plasmon modes at the NW tip, $I_{SPP,0}$. This means that with further careful BlIPP studies, NW in-coupling efficiencies may be experimentally determined. This will be further tested with NWs having different tip geometries.

ASSOCIATED CONTENT

Supporting Information

Additional experimental results. This material is available free of charge via the Internet at http://pubs.acs.org.

AUTHOR INFORMATION

Corresponding Author

*E-mail: slink@rice.edu.

Notes

The authors declare no competing financial interest.

ACKNOWLEDGMENTS

This work was funded by the Robert A. Welch Foundation (C-1664), the Office of Naval Research (N00014-10-1-0989), and NSF (CHE-0955286). D.S. was supported by an NSF Graduate Research Fellowship (Grant No. 0940902). We thank Professor Eugene Zubarev and Leonid Vigderman for supplying the Au NW sample used in these studies.

REFERENCES

(1) Ozbay, E. *Science* **2006**, *311*, 189−193.
(2) Maier, S. A.; Brongersma, M. L.; Kik, P. G.; Meltzer, S.; Requicha, A. A. G.; Atwater, H. A. *Adv. Mater.* **2001**, *13*, 1501−1505.
(3) Dickson, R. M.; Lyon, L. A. *J. Phys. Chem. B* **2000**, *104*, 6095−6098.
(4) Lal, S.; Link, S.; Halas, N. J. *Nat. Photon.* **2007**, *1*, 641−648.
(5) Schuller, J. A.; Barnard, E. S.; Cai, W. S.; Jun, Y. C.; White, J. S.; Brongersma, M. L. *Nat. Mater.* **2010**, *9*, 193−204.
(6) Gramotnev, D. K.; Bozhevolnyi, S. I. *Nat. Photon.* **2010**, *4*, 83−91.
(7) Willingham, B.; Link, S. *Opt. Express* **2011**, *19*, 6450−6461.
(8) Nagpal, P.; Lindquist, N. C.; Oh, S.-H.; Norris, D. J. *Science* **2009**, *325*, 594−597.
(9) Kolomenski, A.; Kolomenskii, A.; Noel, J.; Peng, S. Y.; Schuessler, H. *Appl. Opt.* **2009**, *48*, 5683−5691.
(10) Song, M. X.; Bouhelier, A.; Bramant, P.; Sharma, J.; Dujardin, E.; Zhang, D. G.; Colas-des-Francs, G. *ACS Nano* **2011**, *5*, 5874−5880.
(11) Laroche, T.; Vial, A.; Roussey, M. *Appl. Phys. Lett.* **2007**, *91*, 123101.
(12) Verhagen, E.; Spasenovic, M.; Polman, A.; Kuipers, L. *Phys. Rev. Lett.* **2009**, *102*, 203904.
(13) Pyayt, A. L.; Wiley, B.; Xia, Y. N.; Chen, A.; Dalton, L. *Nat. Nanotechnol.* **2008**, *3*, 660−665.
(14) Soukoulis, C. M.; Wegener, M. *Science* **2010**, *330*, 1633−1634.
(15) Grandidier, J.; Des Francs, G. C.; Massenot, S.; Bouhelier, A.; Markey, L.; Weeber, J. C.; Dereux, A. *J. Microsc.* **2010**, *239*, 167−172.
(16) Li, Z. P.; Bao, K.; Fang, Y. R.; Guan, Z. Q.; Halas, N. J.; Nordlander, P.; Xu, H. X. *Phys. Rev. B* **2010**, *82*, 241402.
(17) Gather, M. C.; Meerholz, K.; Danz, N.; Leosson, K. *Nat. Photon.* **2010**, *4*, 457−461.
(18) Sridharan, D.; Waks, E.; Solomon, G.; Fourkas, J. T. *Appl. Phys. Lett.* **2010**, *96*, 153303.
(19) Ditlbacher, H.; Hohenau, A.; Wagner, D.; Kreibig, U.; Rogers, M.; Hofer, F.; Aussenegg, F. R.; Krenn, J. R. *Phys. Rev. Lett.* **2005**, *95*, 257403.
(20) Ma, Y. G.; Li, X. Y.; Yu, H. K.; Tong, L. M.; Gu, Y.; Gong, Q. H. *Opt. Lett.* **2010**, *35*, 1160−1162.
(21) Wild, B.; Cao, L. N.; Sun, Y. G.; Khanal, B. P.; Zubarev, E. R.; Gray, S. K.; Scherer, N. F.; Pelton, M. *ACS Nano* **2012**, *6*, 472−482.
(22) Ditlbacher, H.; Krenn, J. R.; Felidj, N.; Lamprecht, B.; Schider, G.; Salerno, M.; Leitner, A.; Aussenegg, F. R. *Appl. Phys. Lett.* **2002**, *80*, 404−406.
(23) Solis, D., Jr.; Chang, W.-S.; Khanal, B. P.; Bao, K.; Nordlander, P.; Zubarev, E. R.; Link, S. *Nano Lett.* **2010**, *10*, 3482−3485.
(24) Solis, D., Jr.; Willingham, B.; Nauert, S. L.; Slaughter, L. S.; Olson, J.; Swanglap, P.; Paul, A.; Chang, W.-S.; Link, S. *Nano Lett.* **2012**, *12*, 1349−1353.
(25) Paul, A.; Solis, D., Jr.; Bao, K.; Chang, W. S.; Nauert, S.; Vidgerman, L.; Zubarev, E. R.; Nordlander, P.; Link, S. *ACS Nano* **2012**, *6*, 8105−8113.
(26) Eggeling, C.; Volkmer, A.; Seidel, C. A. M. *ChemPhysChem* **2005**, *6*, 791−804.
(27) Zondervan, R.; Kulzer, F.; Kol'chenko, M. A.; Orrit, M. *J. Phys. Chem. A* **2004**, *108*, 1657−1665.
(28) Dittrich, P. S.; Schwille, P. *Appl. Phys. B: Laser Opt.* **2001**, *73*, 829−837.
(29) Eggeling, C.; Widengren, J.; Rigler, R.; Seidel, C. A. M. *Anal. Chem.* **1998**, *70*, 2651−2659.
(30) Critchley, K.; Khanal, B. P.; Górzny, M. Ł.; Vigderman, L.; Evans, S. D.; Zubarev, E. R.; Kotov, N. A. *Adv. Mater.* **2010**, *22*, 2338−2342.
(31) Chan, Y. H.; Chen, J. X.; Wark, S. E.; Skiles, S. L.; Son, D. H.; Batteas, J. D. *ACS Nano* **2009**, *3*, 1735−1744.
(32) Leong, K.; Chen, Y. C.; Masiello, D. J.; Zin, M. T.; Hnilova, M.; Ma, H.; Tamerler, C.; Sarikaya, M.; Ginger, D. S.; Jen, A. K. Y. *Adv. Funct. Mater.* **2010**, *20*, 2675−2682.
(33) Barnes, W. L. *J. Opt. A: Pure Appl. Opt.* **2006**, *8*, S87−S93.
(34) Staleva, H.; Skrabalak, S. E.; Carey, C. R.; Kosel, T.; Xia, Y. N.; Hartland, G. V. *Phys. Chem. Chem. Phys.* **2009**, *11*, 5889−5896.
(35) Lakowicz, J. R. *Principles of Fluorescence Spectroscopy*, 3 ed.; Springer Science: New York, 2006.
(36) Atkins;, P.; Paula, J. D. *Physical Chemistry For The Life Sciences*, 2 ed.; W. H. Freeman and Company: New York, 2011.
(37) Wennmalm, S.; Rigler, R. *J. Phys. Chem. B* **1999**, *103*, 2516−2519.
(38) Molski, A. *J. Chem. Phys.* **2001**, *114*, 1142−1147.
(39) Yeow, E. K. L.; Melnikov, S. M.; Bell, T. D. M.; De Schryver, F. C.; Hofkens, J. *J. Phys. Chem. A* **2006**, *110*, 1726−1734.

(40) Zondervan, R.; Kulzer, F.; Orlinskii, S. B.; Orrit, M. *J. Phys. Chem. A* **2003**, *107*, 6770−6776.
(41) Berglund, A. J. *J. Chem. Phys.* **2004**, *121*, 2899−2903.
(42) Prummer, M.; Weiss, M. *Phys. Rev. E* **2006**, *74*, 021115.
(43) Fureder-Kitzmuller, E.; Hesse, J.; Ebner, A.; Gruber, H. J.; Schutz, G. J. *Chem. Phys. Lett.* **2005**, *404*, 13−18.